The Role of Various Scattering Mechanisms in $Hg_{1-x}Cd_xTe$ (x=0.22, 0.3)

S. Najafi Bavani[1]; M.S. Akhoundi Khezrabad[2,*]

1- Department of Physics, Payame Noor University (PNU), Tehran, Iran, Email: snajafi2015@gmail.com
2- Department of Physics, Payame Noor University (PNU), Tehran, Iran, Email: ms_akhoundi@pnu.ac.ir

*Corresponding Author
Received: 2020-04-29
Revised: 2020-07-23, 2020-11-01
Accepted: 2021-03-14

Abstract
An iteration computation was carried out to investigate electron transport properties in $Hg_{1-x}Cd_xTe$. We employed the modified iterative procedure which allows us to increase the computational accuracy in several structures. We considered deformation potential, polar optical phonon, piezoelectric, and ionized impurity scattering. Electron drift mobility is calculated for different temperature and doping dependencies. It was found that the electron drift mobility decreases with the temperature increases from 100K to 300K. Competitions among several temperature-dependent scattering mechanisms create temperature-dependent of MCT mobility. Furthermore, it was concluded that the x-dependence of the $Hg_{1-x}Cd_xTe$ mobility results primarily from the x-dependence of bandgap, and secondarily the x-dependence of effective masses. In the case of low temperatures, the electron mobility quickly decreases with the increase of doping concentration, while this happens at a slower speed in the case of high temperatures.

Keywords
Iteration method, electron drift mobility, scattering, $Hg_{1-x}Cd_xTe$.

1. Introduction

IR detectors are widely used in thermal imaging [1,2], material spectroscopy analysis [3-5], autonomous driving assistants [6], surveillance [7], and biological health monitoring [8-11]. The primary photon detector was a PbS detector with a reaction wavelength of 3 µm, and subsequent infrared detectors included germanium-mercury amalgam (Ge: Hg), germanium-silicon combination (Ge: Si), lead selenide (PbSe), indium antimonide (InSb), and mercury cadmium telluride ($Hg_{1-x}Cd_xTe$). The variables, high electron mobility, capacity to obtain both low and high carrier concentrations, direct energy gap, and low dielectric constant are all advantages of HgCdTe. With the advancement of HgCdTe technology, HgCdTe photodetectors are now employed in many application areas, such as night vision [1], chemical sensing [2], space and science imaging [3-5], etc [8-15]. In order to further improve the performance of an electronic and optoelectronic device, it is important to know properties of the carrier transport of semiconductor materials. Theories of carrier transport include nonequilibrium Green's functions [16, 17], the Kubo formalism [18], the Landauer-Buttiker formalism [19, 20, 21], and the Boltzmann transport equation (BTE). Mobility is one of the most essential variables, affecting the current-voltage specifications of the devices. Also, it limits photoconductive gain, dark current, and recombination in photodetectors, including photovoltaic detectors and photo-electromagnetic detectors (PEM) [22-28]. The mobility can be numerically calculated from the solution of the BTE. The Boltzmann transport equation (BTE) has been solved with iterative, finite-difference techniques [29], variational approaches [30], or Monte Carlo sampling [31,32]. This paper aims to calculate the electron mobility in $Hg_{1-x}Cd_xTe$ crystals with x=0.22 and 0.3 in a low electric field by solving the BTE. The goal is achieved through an iteration method. The $Hg_{0.78}Cd_{0.22}Te$ and $Hg_{0.7}Cd_{0.3}Te$ are important to IR detection in atmospheric windows 3-5 µm and 8-12 µm. The iterative method presents a straightforward physical interpretation of the transport equations. Also, the relative simplicity of the formalism allows its generalization to, Fermi statistics, energy band nonparabolicity, n-type and p-type electron wave function admixture, arbitrary time dependence, and combination of various scattering mechanisms. We follow the work of Arabshahi [33-35] and consider in the mobility calculation, the effect of polar-phonon, acoustic, piezoelectric, and ionized impurity scattering. The following is the paper's structure:
Section 2 contains details on the iterative model, as well as electron mobility and scattering rates. The results of iterative calculations carried out on
$Hg_{1-x}Cd_xTe$ structures are offered in Section 3 and were then compared with the theoretical and experimental results of available studies. This is followed by conclusions in Section 4.

2. Theoretical model

The iterative procedure for the calculations is described in Rode [29] that Arabshahi used for binary material and obtained good results in comparison with experimental data. We have used Arabshahi's procedure but improved it so that we can use it for ternary alloy narrow bandgap semiconductors, such as HgCdTe. First, as is the case with HgCdTe, such essential parameters as bandgap, intrinsic concentration, nonparabolity, electron effective mass, hole mass and etc., depending on x and temperature, thus, the number of iterations for convergence was increasing, therefore the programming was carried out thorough the combination of MATLAB and C languages. The modified procedure yielded accurate results for ternary materials. In principle, the iterative technique is an approach to solve the Boltzmann transport equation (BTE) and to obtain the accurate prediction of electron mobility in bulk semiconductors [36]. The Boltzmann equation describes how the electron distribution function evolves under the action of a steady electric field

$$\left(\frac{e}{\hbar}\right)\mathcal{E}.\nabla_k f = \oint [s'f'(1-f) - sf(1-f')]\, d\boldsymbol{k} \quad (1)$$

Where s and f are the differential scattering rates and the probability distribution function ($s = s(\boldsymbol{k}, \boldsymbol{k}')$ and f = f (k)), respectively.

$$f(\boldsymbol{k}) = f_0(\boldsymbol{k}) + g(\boldsymbol{k})\cos\theta \quad (2)$$

θ, $f_0(\boldsymbol{k})$ and $g(\boldsymbol{k})$ are the angle between **k** and Ɛ, the equilibrium distribution function and the isotropic function, respectively and the isotropic function is proportional to the magnitude of the electric field. There are two types of scattering processes to determine contributions to the differential scattering rates. They are elastic scattering, S_{el}, which is because of impurity, acoustic and piezoelectric phonons as well as inelastic scattering, S_{inel}, which is because of polar optic phonons

$$S(\boldsymbol{k}, \boldsymbol{k}') = S_{el}(\boldsymbol{k}, \boldsymbol{k}') + S_{inel}(\boldsymbol{k}, \boldsymbol{k}') \quad (3)$$

The sum of all different elastic scattering rates, such as acoustic, piezoelectric, and ionized impurity scattering, yields the total elastic scattering rate. Sinel is the transition from the state characterized by $\boldsymbol{k}$ to $\boldsymbol{k}'$either by absorption [$S_{ab}(\boldsymbol{k}, \boldsymbol{k}')$] or by emission [$S_{em}(\boldsymbol{k}, \boldsymbol{k}')$] of a phonon. The Boltzmann equation, together with consideration of all differential scattering rates can present us with the factor g(k) in the perturbed part of the distribution function f(k).

$$g(\mathrm{k}) = \frac{\frac{-e\mathcal{E}}{\hbar}\frac{\partial f_0}{\partial k} + \sum_j \int g' \cos\varphi \left[S'_{inelj}(1-f_0) + S_{inelj} f_0\right.}{\sum_i \int (1-\cos\varphi) S_{eli}\, dk' + \sum_j \int \left[S_{inelj}(1-f_0') + S'_{inel}\right.} \quad (4)$$

The first term in the denominator for elastic scattering is the momentum relaxation rate. In the first iteration g(k) is zero. Once g(k) has been estimated to the required precision, it is possible to compute parameters, such as the drift mobility

$$\mu_d = \frac{\hbar}{3m^*}\frac{\int_0^\infty (k^3 g(k)/\mathcal{E}d)dk}{\int_0^\infty k^2 f_0(k)dk} \quad (5)$$

Where d is defined as $1/d = \mathrm{m}^* \nabla_k E/\hbar^2 k$ and ħ, k, and m^* represents the reduced Planck constant, the wave vector and the effective mass [29].

The aim is to calculate the low field drifts mobility in $Hg_{1-x}Cd_xTe$ structure. In the following sections, electron-impurity and electron-phonon mechanisms, including deformation potential scattering, piezoelectric, polar optical phonon scattering, and ionized impurity scattering are taken into account.

2.1. Deformation potential scattering

This mechanism changes the band edge's energy, which is determined by a deformation potential, and the outcome scattering of carriers is called deformation potential scattering. The average value of k (the electron wave-vector) is of the arrange of 10^7*(cm^{-1})* and the velocity of sound (v_s*)* is of the arrange of 10^7 *(cms^{-1})*. Hence, $2\hbar v_s k \sim 1mev$, which is insubstantial compared to the thermal energy at room temperature. For this reason, the deformation potential scattering of acoustic modes can be considered as an elastic process however at very low temperatures. The deformation potential scattering rate with both phonon absorption or emission for an electron of energy E in a nonparabolic band is described via Fermi's golden rule.

$$S_{ab}(E) = \frac{\sqrt{2}D_{ac}^2 (m^*)^{3/2} K_B T}{\pi\rho v^2 \hbar^4} \times \frac{\sqrt{E(1+\alpha E)}}{(1+2\alpha E)} \quad (6)$$

$$[(1+\alpha E)^2 + 1/3(\alpha E)^2]$$

where D_{ac}, K_B, α, ρ and T are the deformation potential, Boltzmann constant, nonparabolicity coefficient of the conduction band, the material density, and lattice temperature, respectively. This formula illustrates that the acoustic scattering increases with temperature [37-39]. The curve a in Fig. 1 shows that energy increase causes acoustic phonon scattering increasing and also show the acoustic phonon scattering rate of $Hg_{0.7}Cd_{0.3}Te$ is more than $Hg_{0.78}Cd_{0.22}Te$, due to a larger amount of electron effective mass in $Hg_{0.7}Cd_{0.3}Te$.

2.2. Polar optical phonon scattering

The dipolar electric field arising from the contrary displacement of the negatively and positively charged atoms makes a coupling between the electrons and the lattice which ultimately results in electron scattering. This scattering is called polar optical phonon scattering and is commonly the most significant scattering mechanism for electrons in II-VI semiconductors at room temperature. As a result, the scattering rate for an electron of energy E in the isotropic, nonparabolic band is $R_{po}(\vec{E})$ where N_{op} is the phonon occupation number.

$$R_{po}(\vec{E}) = \frac{e^2\sqrt{2m^*}\omega_{op}}{8\pi\varepsilon_\circ\hbar}\left(\frac{1}{\varepsilon_\infty} - \frac{1}{\varepsilon_s}\right) \quad (7)$$

$$\frac{(1+2\alpha E')}{\sqrt{\gamma(E)}} F_o(E, E')\{N_{op}, N_{op}+1\}$$

Now,

$$E' = \begin{cases} E + \hbar\omega_{op} & (absorption) \\ E - \hbar\omega_{op} & (emission) \end{cases} \quad (8)$$

is the final energy state in a phonon absorption (upper case) and a phonon emission (lower case) where $\hbar w_{op}$ is the polar optical phonon energy. The other quantities are read as

$$F_0(E,E') = C^{-1}\left\{ A\, ln\left|\frac{\gamma(E)^{\frac{1}{2}} + \gamma(E')^{\frac{1}{2}}}{\gamma(E)^{\frac{1}{2}} - \gamma(E')^{\frac{1}{2}}}\right| + B\right\} \quad (9)$$

$$A = [2(1+\alpha E)(1+\alpha E') + \alpha(\gamma+\gamma')]^2 \quad (10)$$

$$B = -2\alpha\gamma^{\frac{1}{2}}\gamma'^{\frac{1}{2}} \; [4(1+\alpha E)(1+\alpha E') + \alpha(\gamma+\gamma')] \quad (11)$$

$$C = 4(1+\alpha E)(1+\alpha E') \; (1+2\alpha E)(1+2\alpha E') \quad (12)$$

At room temperature, polar optical phonon scattering dominates in the Γ-valley.

The polar optical phonon scattering rate (emission) happens when the electron energy is more than the optical phonon energy. The average number of photons is given by the Bose-Einstein distribution

$$N_{op} = \frac{1}{exp\left(\frac{\hbar\omega_{op}}{K_B T}\right) - 1} \quad (13)$$

$\hbar w_{op}$ is the polar optical phonon energy [37-39]. The curve b in Fig. 1 does not start with zero because the polar optical phonon scattering (emission) happens when the electron energy is more than $\hbar\omega_{op}$ but the curve d in Fig. 1 starts with zero since the polar optical phonon scattering (absorption) phenomenon occurs for all materials with any level of energy for electrons.

The curve b in Fig. 1 showing the polar optical phonon scattering is generally the most important scattering mechanism for electrons at room temperature. At this temperature, the phonon occupation number is so excessive that the polar optical phonon scattering rate (emission) dominates in a wide variety of energy. Also, the polar optical phonon scattering rate of $Hg_{0.7}Cd_{0.3}Te$ is more than $Hg_{0.78}Cd_{0.22}Te$ due to its large amount of nonparabolicity coefficient.

2.3. Intravalley impurity scattering

The Brook-Herring (BH) technique is the standard method for numerical calculation of the ionized impurity scattering in semiconductors [40]. To overcome the Born approximation, the BH method has proven that the phase-shift analysis of electron-impurity scattering is the best method. At high electron concentrations, the departure from the BH predictions of electron mobility is obvious. Bartoli and Meyer have considered analytic dealing relying on the phase-shift analysis taking into consideration the multi-ion screening effect [37-40]. All the previous methods of impurity screening with free electrons in semiconductors were based on the Thomas- Fermi (TF) approximation. This approximation assures that a given impurity should be fully screened. The single-ion screening formalism becomes less related at high compensation. This is because to maintain the charge neutrality situation, it will be more difficult for a given number of electrons to screen all the ionized donors separately. The compensation ratio for $Hg_{1-x}Cd_xTe$ is usually quite large, and the ratio N_D^+/n is also temperature-dependent. Hence the multi-ion screening modification is very necessary for $Hg_{1-x}Cd_xTe$. Thus, we have used phase-shift analysis to calculate the differential scattering rate (k,k'). The effective potential V(r) can be given as: $V(r) = -(Z_l e^2)/(4\pi\varepsilon_0 k_0 r)e^{-r/\lambda}$, where λ is the screening length and Z_l is the charge of the ionized impurity in units of e. For obtaining the screening length, we use the TF approach which is based on single ion screening approximation. The TF approach can calculate the charge contribution q_i to the screening of a single ionized donor by an electron of energy E_i and is given by

$q_i = -(2e^3\lambda^2/\varepsilon_0 k_0 E_i V)$ also, for the multi-ion, the TF method can be expressed as: $Q_i = -(2e^3\lambda^2 N_D^+/\varepsilon_0 k_0 E_i)$.

$$\sum_i -\frac{Q_i}{e} f_0(E_i) = N_D^+ \quad (14)$$

For enough low energy electrons, Q_i can be greater than the electronic charge, which is physically illogical. One way to solve this problem is to recommend a factor S_i such as

$$S_i(E_i) = \frac{E_i}{\xi} \quad (15)$$

And Qi will be corrected as $Q_i' = Q_i S_i$ in equation 14 and $\xi = (2c^2\lambda^2 N_D^+/\varepsilon_0 k_0)$. The contribution will be –e for the low energy electrons. Since the total contribution to the screening by the low energy electrons has been effectively decreased, equation 14 no longer holds. However, in case the screening length λ is more than the average distance between the donors, donors may not be needed to be fully screened as the preservation of totally charge neutrality suffices. Electrons in the overlap region can supply screening with the ionized donors. In the equation 14, factor p would be the fraction of the total charge and factor p is included within a sphere of radius R surrounding the donor. Therefore, equation 14 will be modified as

$$\sum_i -\frac{Q_i^{"}}{e} f_0(E_i) = pN_D^+ \quad (16)$$

Where $Q_i^{"} = pQ_i S_i$

$$\lambda_m^{-2} = \eta\lambda_0^{-2} \quad (17)$$

Where λ_0, and λ_m are TF screening length, and multi-ion screening length, respectively. The equation for the ionized impurity scattering rate

$$S_{ii}(k,k') = \frac{8\pi^3\hbar^3}{m^{*2}V^2}|f(x)|^2 \quad (18)$$

$\delta[E(K') - E(K)]$

the scattering amplitude *f(x)* depends on Legendre polynomial P_1 and the phase shift $\delta_1$and is written by

$$f(X) = \frac{1}{2ik}\sum_{l=0}^{\infty}(2l+1)\left(e^{2i\delta_l}-1\right)P_l(X) \quad (19)$$

The curve c in Fig. 1 demonstrates that the ionized impurity scattering rate decreases with energy increasing because electrons energy increase can lead to the electron velocity increase and the Coulomb screening potential. The reason can be ascribed to impurity atoms effects on the electrons in a shorter time. Therefore, ionized impurity scattering is important for carrier transport at low electric fields and temperature.

2.4. Piezoelectric scattering

The piezoelectric scattering can happen in the compound semiconductors, such as the II-VI and III-V materials. $Hg_{1-x}Cd_xTe$ is a part of these materials. It is worth noting that $Hg_{1-x}Cd_xTe$ has a relatively large piezoelectric constant. Ridley [38] has considered the piezoelectric scattering rate for an electron of energy E in the isotropic, nonparabolic band. He also considered the modification of the Coulomb potential because free carrier screening. The screened Coulomb potential is given as

$$V(r) = \frac{e^2}{4\pi\varepsilon_0\varepsilon_s}.\frac{exp(-q_0 r)}{r} \quad (20)$$

Where q_0 and ε_s are the inverse screening length and the relative dielectric constant of the material respectively, which under non-degenerate conditions are written by

$$q_0^2 = \frac{ne^2}{\varepsilon_0\varepsilon_s k_B T} \quad (21)$$

n is the electron density. The equation for the scattering rate of an electron in a non-parabolic band structure retaining the essential terms can be given as

$$R_{pz}(E) = \frac{\sqrt{m^*}e^2K_{ac}^2K_BT}{4\sqrt{2}\pi\hbar^2\varepsilon_0\varepsilon_s}\gamma^{-1/2}(E)(1+2\alpha E)^2 \times\left[\ln\left(1+\frac{8m^*\gamma(E)}{\hbar^2q_0^2}\right) - \frac{1}{1+\hbar^2q_0^2/8m^*\gamma(E)} + \left(\frac{\sqrt{2}\alpha E}{1+2\alpha E}\right)^2\right] \quad (22)$$

Where K_{ac} is the average electromechanical coupling constant and it is dimensionless.

$$\gamma(E) = E(1+\alpha E) = \frac{\hbar^2 k^2}{2m^*} \quad (23)$$

, with

$$\alpha = \frac{1}{E_g}\left(1-\frac{m^*}{m_0}\right)^2 \quad (24)$$

In energy-wave vector relation, E is the electron energy in the conduction band, E_g is the bandgap of the material, and m_0 is the mass of free electrons [38]. The curve a in Fig. 2 showing the piezoelectric scattering rate only matters in low energy. Also, the piezoelectric scattering rate of $Hg_{0.7}Cd_{0.3}Te$ is more than $Hg_{0.78}Cd_{0.22}Te$, due a larger electromechanical coupling constant and a lower amount of the inverse screening length and nonparabolicity coefficient in $Hg_{0.7}Cd_{0.3}Te$.

Table I. Parameters of $Hg_{1-x}Cd_xTe$, is used in the iterative method [41-45].

	Unit	x (Molar Cd)		
		0.22	0.3	Ref.
v	ms^{-1}	2054	2077	[41,44]
ρ	kgm^{-3}	7544	7360	[41,44]
$\varepsilon_\circ$	-	17.34	16.33	[41,44]
ε_∞	-	12.16	11.25	[41,44]
D_{ac}	ev	9.47	9.45	[41,44]
ω_{op}	ev	0.0183	0.0184	[41,44]
a	Å	6.4640	6.4653	[41,4∘]
p	Ccm^{-2}	0.028	0.029	[41,42]
α	ev^{-1}	5.3515	3.2992	Calc.
E_g	ev	0.1819	0.2906	[41]
m^*	-	0.0134	0.0209	[41]

3. Result and Discussion

Building on the iteration method, the scattering rates and mobility of $Hg_{0.78}Cd_{0.22}Te$ and $Hg_{0.7}Cd_{0.3}Te$ were studied. The main scattering parameters, which were employed in this method, are reported in Table I. Fig. 1 and Fig. 2 show the energy dependence of scattering rate in $Hg_{1-x}Cd_xTe$ for x = 0.22 and 0.3. In curves, the carrier concentration is taken to be $n = 10^{17}cm^{-3}$ for x=0.22 and $n = 10^{16}cm^{-3}$ for x=0.3 at 300K. In order to understand which scattering mechanisms limit the mobility of $Hg_{1-x}Cd_xTe$ under various conditions, we have separately performed calculations of the scattering mechanisms. Fig. 1 and Fig. 2 show the calculated scattering for all scattering mechanisms. The curve (b) in Fig. 2 shows the calculated scattering for all scattering mechanisms. This should be noted that Ionized impurity scattering is important since it is primarily dominant in the case of low-energy carriers and then the polar optical phonon (emission) scattering becomes dominant in more energies. Thus, the marked reduction in mobility can be ascribed to the polar optical phonon (emission) scattering. We performed low-field electron mobility calculations in $Hg_{1-x}Cd_xTe$ structures. Using the iteration method low field mobility has been derived.

Fig. 3 shows the temperature dependence of electron drift mobility in $Hg_{1-x}Cd_xTe$ for x = 0.22 and 0.3. According to Fig. 3, the electron drift mobility decreases with the increasing temperature because the optical phonon scattering rate increase. The variation of the mobility curve as a function of temperature shows how different scattering mechanisms compete with each other in the different temperature ranges. In between 5-100 K, the ionized impurity scattering is a dominant mechanism and the electron mobility shows a maximum value at about 50 K and the polar optical-phonon scattering is dominant because of the temperature increase and its mobility begins to decrease quickly. Nevertheless, the competition between different scattering mechanisms in case of x=0.3 is not serious in comparison with x=0.2, because its slope of the curve is less than x=0.22 and the difference between their band structure and effective mass can be another reason. Studies with a focus on the effect of doping in mobility can significantly contribute to electronic and optoelectronic device design.

Fig. 4 illustrates the variation of electron mobility in terms of concentration in T=77, 150 and 300K for bulk $Hg_{0.78}Cd_{0.22}Te$ (a) and $Hg_{0.7}Cd_{0.3}Te$ (b). In curve (a), the intrinsic carrier concentration is taken to be $n_i(0.22,77) = 10^{13}cm^{-3}, n_i(0.22,150) = 10^{15}cm^{-3}, n_i(0.22,300) = 10^{16}cm^{-3}$ and in curve (b), the intrinsic carrier concentration is taken to be $n_i(0.3,77) = 10^{9}cm^{-3}, n_i(0.3,150) = 10^{13}cm^{-3}$, $n_i(0.3,300) = 10^{15}cm^{-3}$. The results plotted in Fig. 4 indicate that electron drift mobility decreases with any increase in donor concentration. For the lower temperature case, the electron drift mobility decreases faster than the higher temperature cases because of the temperature dependence on intrinsic carrier concentration ni. In this situation, the ratio of doping concentration to intrinsic concentration ($Z_x^T = \frac{N_d}{n_i(x,T)}$) is determined. Z is a measure for the doping regime, the less Z_x^T means low doping and the more Z_x^T means highly doping. It is noticeable that the mobility in 77K is less than mobility in 150 and 300K in the range $10^{17} - 10^{18}cm^{-3}$ because Z_x^{77} is more than Z_x^{150} and Z_x^{300} in both $Hg_{0.78}Cd_{0.22}Te$ and $Hg_{0.7}Cd_{0.3}Te$. The mobility variation for the curve of 300K respects the doping change is less than two other curves because of the Z_x^{300} variation is less than Z_x^{150} and Z_x^{77}.

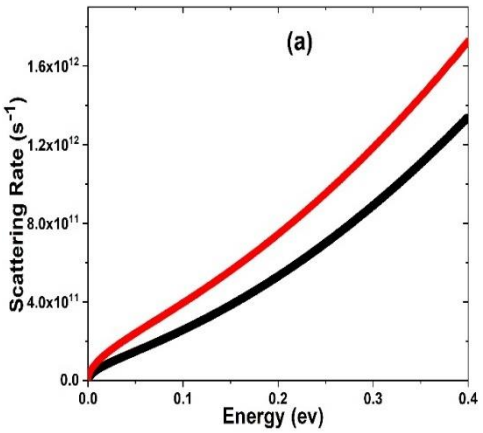

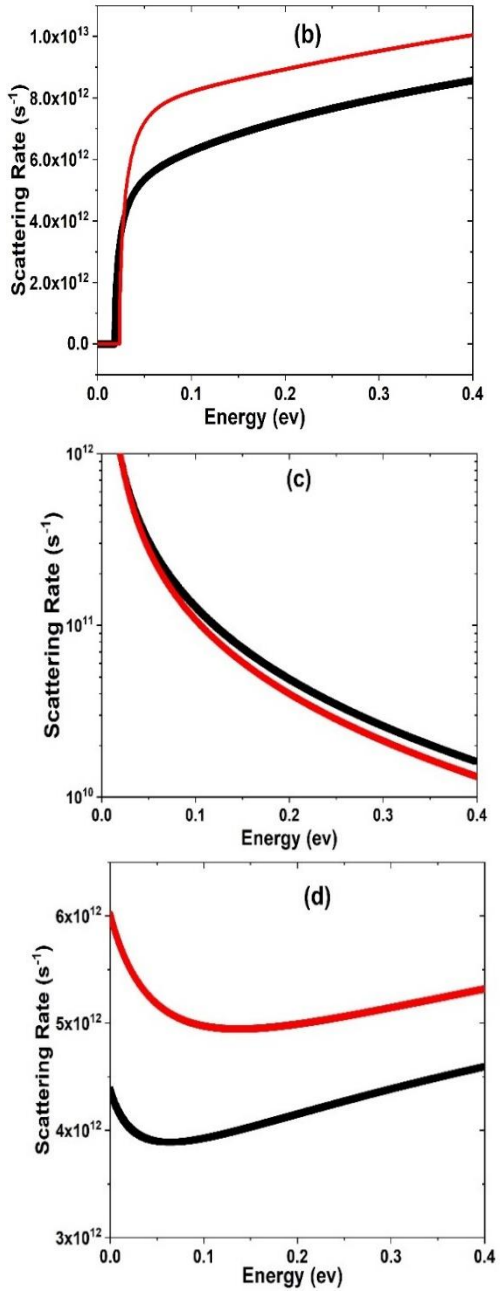

Fig. 1. Calculated electron scattering rates as a function of energy for bulk $Hg_{0.78}Cd_{0.22}Te$ (black line) and $Hg_{0.7}Cd_{0.3}Te$ (red line) at T = 300 K and the carrier concentration is taken to be $n = 10^{17}cm^{-3}$ for x=0.22 and $n = 10^{16}cm^{-3}$ for x=0.3 :(a) acoustic phonon (b) polar-optical phonon (emission) (c) ionized impurity (d) polar-optical phonon (absorption).

Although increasing doping causes the increasing scattering center and decreasing mobility, Z is the determinant factor that is dependent on temperature and ratio of impurity concentration to intrinsic concentration. Also, as can be observed in Fig. 4(a), although doping for curves in the point of intersection is almost $10^{17}cm^{-3}$, their Z_x^T are different, where $Z_{0.22}^{77}$, $Z_{0.22}^{150}$, and $Z_{0.22}^{300}$ are 10^4, 10^2 and 10^1, respectively, and they correspond to highly, medium and near intrinsic doping. Thus, it is advisable to study mobility as a function of Z_x^T, instead of doping concentration. Similar behaviour is seen in Fig. 4(b).

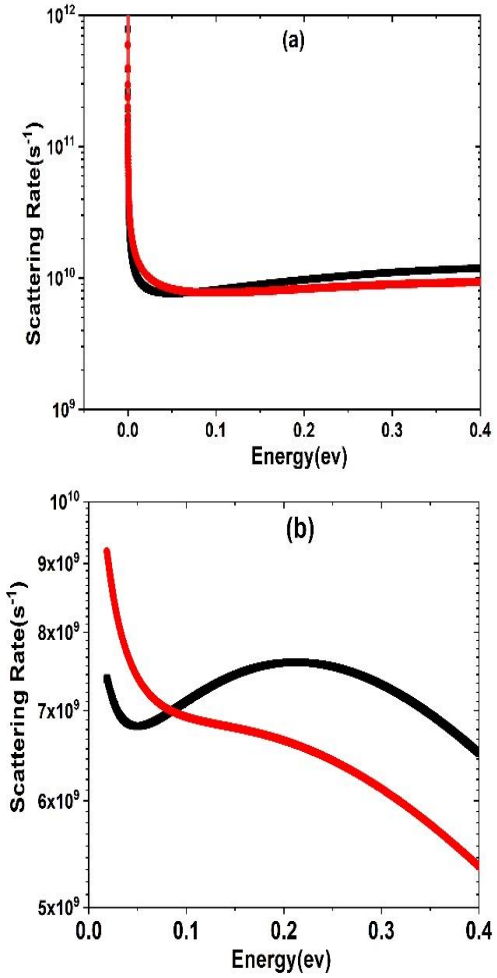

Fig. 2. Calculated electron scattering rates as a function of energy for bulk $Hg_{0.78}Cd_{0.22}Te$ (black line) and $Hg_{0.7}Cd_{0.3}Te$ (red line) at T = 300 K and the carrier concentration is taken to be $n = 10^{17} cm^{-3}$ for x=0.22 and $n = 10^{16} cm^{-3}$ for x=0.3 :(a) piezoelectric (b) total scattering rate.

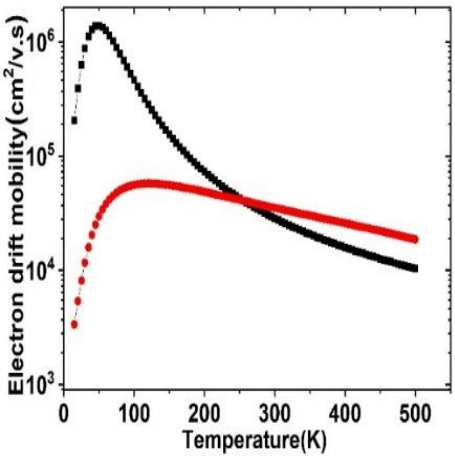

Fig. 3-The electron mobility versus temperature for bulk $Hg_{0.78}Cd_{0.22}Te$ (black line) and $Hg_{0.7}Cd_{0.3}Te$ (red line) from 10K to 500 K and the carrier concentration is taken to be $n = 10^{17} cm^{-3}$ for x=0.22 and $n = 10^{16} cm^{-3}$ for x=0.3.

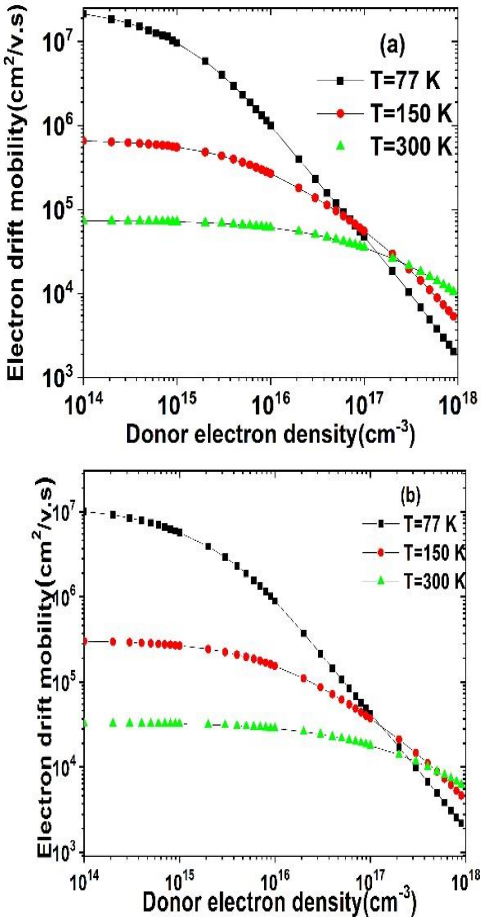

Fig. 4. Variations of electron mobility in terms of concentration in T=77, 150 and 300K for bulk $Hg_{0.78}Cd_{0.22}Te$ (a) and $Hg_{0.7}Cd_{0.3}Te$ (b).

Moreover, we compared our results with numerical results Yoo [46], Miles [47], Higgins [48] et al and experimental results Bartoli [49], Nimtz [50], Scott [51], Mroczkowski [52], and Wu [53] et al that you can see some of them in Table II.

This comparison shows a reasonable discrepancy. This is because, in study (46), carrier density at temperature 300K was mentioned 10^{15} cm^{-3} (Z=0.1) with the compensation ratio 0.2 while we have chosen 10^{16} cm^{-3} (Z=10). Also, in references (45), (44), and (48), annealed samples are used. In this case, the compensation and the iconicity of impurities should be considered. The compensation causes a change in the real carrier density, followed by a change in mobility. In addition, n times changing in ionicity result in n^2 times changing in impurity scattering strength [45,54]. As HgCdTe is an II-VI compound matter, the impurity may be divalent. Divalent ionicity enhances impurity scattering strength four times. Thus, it is noticeable that our results are larger than the values compared to them.

4. Conclusions

In conclusion, drawing on the iterative method in the low applied field, we calculated the electron transport characteristic related to zincblende $Hg_{1-x}Cd_xTe$ structures.

Table II. Comparison of current Study results with other Studies.

x	T(k)	Mobility	Ref.
0.22	77	8.2×10^5	This work
0.22	77	2.1×10^5	[44]
0.22	77	1.8×10^5	[47]
0.22	77	1.1×10^4	[48]
0.22	77	1.9×10^5	[49]
0.22	300	2.8×10^4	This work
0.22	300	0.8×10^4	[44]
0.22	300	1.0×10^4	[47]
0.22	300	1.7×10^5	[48]
0.22	300	1.4×10^4	[49]
0.3	77	4.8×10^4	This work
0.3	77	5.8×10^4	[44]
0.3	77	6.0×10^4	[47]
0.3	77	4.0×10^4	[50]
0.3	77	3.6×10^4	[51]
0.3	300	3.5×10^4	This work
0.3	300	5.0×10^4	[44]
0.3	300	4.0×10^4	[47]
0.3	300	5.6×10^3	[46]
0.3	300	6.3×10^3	[45]

According to our calculation, as depicted in Fig. 1 and Fig. 2, all scattering rates are dependent on x because of the bandgap dependence of x except ionized impurity and piezoelectric scattering rates. Moreover, the polar optical phonon (emission) scattering is prevailing in the energy range 0.05-0.4 *(ev)*. We obtained temperature dependence in the mobility results from the competition among various scattering mechanisms, which are temperature-dependent. At low temperature, the ionized impurity scattering is a dominant mechanism and the electron mobility shows a maximum value at about 50 K. Then the polar optical-phonon scattering is dominant because of temperature increase and its mobility begins to decrease quickly. However, the competition between different scattering mechanisms in case of x=0.3 is not serious in comparison with x=0.2, because its slope of the curve is less than x=0.22. It was found that the low-field electron mobility is significantly higher for the $Hg_{1-x}Cd_xTe$ structures with lower x because of primarily the x-dependence of bandgap, and secondarily the x-dependence of effective masses. Z_x^T is a simple criterion for the interpretation of the dependent simultaneous mobility to doping and temperature. Finally, the results our study were in a good agreement with those of the existing literature.

References

[1] A. Rogalski, "Toward third generation HgCdTe infrared detectors," Journal of alloys and compounds, vol. 371, no. 1-2, pp. 53-57, 2004.

[2] A. Rogalski, J. Antoszewski, and L. Faraone, "Third-generation infrared photodetector arrays," Journal of applied physics, vol. 105, no. 9, pp. 4, 2009.

[3] J. W. Stouwdam, and F. C. van Veggel, "Near-infrared emission of redispersible Er3+, Nd3+, and Ho3+ doped LaF3 nanoparticles," Nano letters, vol. 2, no. 7, pp. 733-737, 2002.

[4] J. Schmitt, and H.-C. Flemming, "FTIR-spectroscopy in microbial and material analysis," International Biodeterioration & Biodegradation, vol. 41, no. 1, pp. 1-11, 1998.

[5] J. Madejová, "FTIR techniques in clay mineral studies," Vibrational spectroscopy, vol. 31, no. 1, pp. 1-10, 2003.

[6] A. González, Z. Fang, Y. Socarras, J. Serrat, D. Vázquez, J. Xu, and A. M. López, "Pedestrian detection at day/night time with visible and FIR cameras: A comparison," Sensors, vol. 16, no. 6, pp. 820, 2016.

[7] S. Briz, A. De Castro, J. Aranda, J. Meléndez, and F. López, "Reduction of false alarm rate in automatic forest fire infrared surveillance systems," Remote Sensing of Environment, vol. 86, no. 1, pp. 19-29, 2003.

[8] R. Soref, "Mid-infrared photonics in silicon and germanium," Nature photonics, vol. 4, no. 8, pp. 495-497, 2010.

[9] L. Miller, G. Smith, and G. Carr, "Synchrotron-based biological microspectroscopy: from the mid-infrared through the far-infrared regimes," Journal of Biological Physics, vol. 29, no. 2, pp. 219-230, 2003.

[10] T. Yokota, P. Zalar, M. Kaltenbrunner, H. Jinno, N. Matsuhisa, H. Kitanosako, Y. Tachibana, W. Yukita, M. Koizumi, and T. Someya, "Ultraflexible organic photonic skin," Science advances, vol. 2, no. 4, pp. e1501856, 2016.

[11] N. Nelms, and J. Dowson, "Goldblack coating for thermal infrared detectors," Sensors and Actuators A: Physical, vol. 120, no. 2, pp. 403-407, 2005.

[12] O. Salvetti, L. A. Ronchi, C. Corsi, A. Rogalski, and M. Strojnik, "Advanced infrared technology and applications," Advances in Optical Technologies, vol. 2013, pp. 1-2, 2013.

[13] A. Rogalski, M. Kopytko, and P. Martyniuk, "Performance prediction of pin HgCdTe long-wavelength infrared HOT photodiodes," Applied optics, vol. 57, no. 18, pp. D11-D19, 2018.

[14] I. Izhnin, K. Mynbaev, A. Voitsekhovskii, S. Nesmelov, S. Dzyadukh, A. Korotaev, V. Varavin, S. Dvoretsky, D. Marin, and M. Yakushev, "Electrical and microscopic characterization of p+-type layers formed in HgCdTe by arsenic implantation," Semiconductor Science and Technology, vol. 35, no. 11, pp. 115019, 2020.

[15] I. I. Izhnin, K. D. Mynbaev, A. V. Voytsekhovskiy, S. N. Nesmelov, S. M. Dzyadukh, O. I. Fitsych, V. S. Varavin, S. A. Dvoretsky, N. N. Mikhailov, and A. Korotaev, "Hall-effect studies of modification of

HgCdTe surface properties with ion implantation and thermal annealing," 2020.
[16] L. Kadanoff, and G. Baym, "Quantum Statistical Mechanics, Benjamin, New York (1962)," 1989.
[17] L. V. Keldysh, "Diagram technique for nonequilibrium processes," Sov. Phys. JETP, vol. 20, no. 4, pp. 1018-1026, 1965.
[18] R. Kubo, "The fluctuation-dissipation theorem," Reports on progress in physics, vol. 29, no. 1, pp. 255, 1966.
[19] R. Landauer, "Can a length of perfect conductor have a resistance?," Physics Letters A, vol. 85, no. 2, pp. 91-93, 1981.
[20] M. Büttiker, "Four-terminal phase-coherent conductance," Physical review letters, vol. 57, no. 14, pp. 1761, 1986.
[21] R. Landauer, "Conductance determined by transmission: probes and quantised constriction resistance," Journal of Physics: Condensed Matter, vol. 1, no. 43, pp. 8099, 1989.
[22] P. Martyniuk, M. Kopytko, and A. Rogalski, "Barrier infrared detectors," Opto-electronics review, vol. 22, no. 2, pp. 127-146, 2014.
[23] M. Karimi, M. Kalafi, and A. Asgari, "Numerical optimization of an extracted HgCdTe IR-photodiodes for 10.6-μm spectral region operating at room temperature," Microelectronics journal, vol. 38, no. 2, pp. 216-221, 2007.
[24] E. Melezhik, J. Gumenjuk-Sichevska, and F. Sizov, "Electron mobility in semi-metal HgCdTe quantum wells: dependence on the well width," SpringerPlus, vol. 5, no. 1, pp. 1-10, 2016.
[25] انوری فرد.م, "انسداد میدان الکتریکی جانبی از نواحی درین و سورس جهت بهبود اثرات کانال کوتاه در افزاره .Nano-SOI",مجله مهندسی برق دانشگاه تبریز, vol. 48, no. 3, pp. 991-998, ۱۳۹۷.
[26] صیفوری. م, امیری .پ, داردس. ا, "تقویت‌کننده الکترونیکی مقاومت انتقالی برای شبکه‌های مخابرات نوری با ساختار جدید مبتنی بر پسخور فعال ولتاژ جریان ", .مجله مهندسی برق دانشگاه تبریز .vol , 48, no.2, pp.737-744, ۱۳۹۷.
[27] M. Kopytko, A. Kębłowski, P. Madejczyk, P. Martyniuk, J. Piotrowski, W. Gawron, K. Grodecki, K. Jóźwikowski, and J. Rutkowski, "Optimization of a HOT LWIR HgCdTe photodiode for fast response and high detectivity in zero-bias operation mode," Journal of Electronic Materials, vol. 46, no. 10, pp. 6045-6055, 2017.
[28] B. BARUTCU, "DEVELOPMENT OF HIGH PERFORMANCE LONG WAVELENGTH INFRARED HGCDTE FOCAL PLANE ARRAYS," MIDDLE EAST TECHNICAL UNIVERSITY, 2019.
[29] D. Rode, "Low-field electron transport," Semiconductors and semimetals, pp. 1-89: Elsevier, 1975.
[30] H. Ehrenreich, "Band structure and transport properties of some 3–5 compounds," Journal of Applied Physics, vol. 32, no. 10, pp. 2155-2166, 1961.
[31] S. Smirnov, H. Kosina, M. Nedjalkov, and S. Selberherr, "A zero field Monte Carlo algorithm accounting for the pauli exclusion principle." pp. 185-193,2003.
[32] S. Derelle, S. Bernhardt, R. Hardar, J. Primot, J. Deschamps, and J. Rothman, "A Monte Carlo Study of $\hbox {Hg} _ {0.7}\hbox {Cd} _ {0.3}\hbox {Te} $ e-APD," IEEE transactions on electron devices, vol. 56, no. 4, pp. 569-577, 2009.
[33] H. Arabshahi, "Simulations of electron transport in GaN devices," Durham University, 2002.
[34] H. Arabshahi, and A. Mowlavi, "Low-field electron transport properties in zincblende and wurtzite GaN structures using an iteration model for solving Boltzmann equation," Modern Physics Letters B, vol. 23, no. 10, pp. 1359-1366, 2009.
[35] H. Arabshahi, "Calculation of Electron Hall Mobility in GaSb, GaAs and GaN Using an Iterative Method," The African Review of Physics, vol. 2, no. 1, 2009.
[36] S. Poncé, W. Li, S. Reichardt, and F. Giustino, "First-principles calculations of charge carrier mobility and conductivity in bulk semiconductors and two-dimensional materials," Reports on Progress in Physics, vol. 83, no. 3, pp. 036501, 2020.
[37] C. Jacoboni, Theory of electron transport in semiconductors: a pathway from elementary physics to nonequilibrium Green functions: Springer Science & Business Media, 2010.
[38] B. K. Ridley, Electrons and phonons in semiconductor multilayers: Cambridge University Press, 2009.
[39] M. L. Cohen, and J. R. Chelikowsky, Electronic structure and optical properties of semiconductors: Springer Science & Business Media, 2012.
[40] H. Brooks, "Scattering by ionized impurities in semiconductors." pp. 879-879,1951.
[41] K. F. Brennan, and N. S. Mansour, "Monte Carlo calculation of electron impact ionization in bulk InAs and HgCdTe," Journal of applied physics, vol. 69, no. 11, pp. 7844-7847, 1991.
[42] J. Meyer, and F. Bartoli, "Low-temperature electron transport in GaAs," Solid State Communications, vol. 41, no. 1, pp. 19-22, 1982.

[43] H. Koçer, "Numerical modeling and optimization of HgCdTe infrared photodetectors for thermal imaging," 2011.

[44] R. Yadava, A. Gupta, and A. Warrier, "Hole scattering mechanisms in Hg 1− x Cd x Te," Journal of electronic materials, vol. 23, no. 12, pp. 1359-1378, 1994.

[45] J. Dubowski, T. Dietl, W. Szymańska, and R. Gałazka, "Electron scattering in CdxHg1− xTe," Journal of Physics and Chemistry of Solids, vol. 42, no. 5, pp. 351-362, 1981.

[46] S. D. Yoo, and K. D. Kwack, "Theoretical calculation of electron mobility in HgCdTe," Journal of applied physics, vol. 81, no. 2, pp. 719-725, 1997.

[47] R. Miles, "A6. 4 Electron and hole mobilities in HgCdTe," Properties of Narrow Gap Cadmium-based compounds, no. 10, pp. 221, 1994.

[48] W. Higgins, G. Pultz, R. Roy, R. Lancaster, and J. Schmit, "Standard relationships in the properties of Hg1− x Cd x Te," Journal of Vacuum Science & Technology A: Vacuum, Surfaces, and Films, vol. 7, no. 2, pp. 271-275, 1989.

[49] F. Bartoli, J. Meyer, C. Hoffman, and R. Allen, "Electron mobility in low-temperature Hg 1− x Cd x Te under high-intensity C O 2 laser excitation," Physical Review B, vol. 27, no. 4, pp. 2248, 1983.

[50] G. Nimtz, G. Bauer, R. Dornhaus, and K. Müller, "Transient carrier decay and transport properties in Hg 1− x Cd x Te," Physical Review B, vol. 10, no. 8, pp. 3302, 1974.

[51] W. Scott, "Electron Mobility in Hg1− x Cd x Te," Journal of Applied Physics, vol. 43, no. 3, pp. 1055-1062, 1972.

[52] J. Mroczkowski, J. Shanley, M. Reine, P. LoVecchio, and D. Polla, "Erratum: Lifetime measurement in Hg0. 7Cd0. 3Te by population modulation," Applied Physics Letters, vol. 38, no. 12, pp. 1033-1033, 1981.

[53] T. Wu, K. Lam, C. Chiang, J. Gong, and S.-J. Yang, "Activation of boron implanted in Hg0. 7Cd0. 3Te by high-temperature annealing," Journal of applied physics, vol. 63, no. 10, pp. 4983-4988, 1988.

[54] S. N. Bavani, and M. A. Khezrabad, "The electron mobility in Hg1-xCdxTe (x= 0.22 and 0.3): A comparison between experimental and theoretical results," Materials Research Bulletin, vol. 140, pp. 111325, 2021.